

The Effect of Cooling on the Density Profile of Hot Gas in Clusters of Galaxies: Is Additional Physics Needed?

Tatsushi Suginozara^{1,2,3} and Jeremiah P. Ostriker⁴

Department of Astrophysical Sciences, Princeton University, Princeton, NJ 08544

ABSTRACT

We use high-resolution hydrodynamic simulations to investigate the density profile of hot gas in clusters of galaxies, adopting a variant of cold dark matter cosmologies and employing a cosmological N-body/smoothed particle hydrodynamics code to follow the evolution of dark matter and gas. In addition to gravitational interactions, gas pressure, and shock heating, we include bremsstrahlung cooling in the computation. Dynamical time, two-body relaxation time, and cooling time in the simulations are examined to demonstrate that the results are free from artificial relaxation effects and that the time step is short enough to accurately follow the evolution of the system. In the simulation with nominal resolution of $66h^{-1}$ kpc the computed cluster appears normal, but in a higher (by a factor 2) resolution run, cooling is so efficient that the final gas density profile shows a steep rise toward the cluster center that is not observed in real clusters. Also, the X-ray luminosity of 7×10^{45} ergs s^{-1} far exceeds that for any cluster of the computed temperature. The most reasonable explanation for this discrepancy is that there are some physical processes still missing in the simulations that actually mitigate the cooling effect and play a crucial role in the thermal and dynamical evolution of the gas near the center. Among the promising candidate processes are heat conduction and heat input from supernovae. We discuss the extent to which these processes can alter the evolution of gas.

Subject headings: cosmology: miscellaneous — galaxies: clusters: general — hydrodynamics — intergalactic medium — methods: numerical

The Astrophysical Journal, 507, 16 (1998)

¹Department of Physics, the University of Tokyo, Tokyo 113, Japan

²RESCEU, School of Sciences, the University of Tokyo, Tokyo 113, Japan

³tatsushi@astro.Princeton.EDU, JSPS Postdoctoral Fellow

⁴jpo@astro.Princeton.EDU

1. Introduction

Hot X-ray-emitting gas in clusters of galaxies contains a variety of information relevant to many fields in astrophysics. Density and temperature profiles of the gas give among the most reliable estimates of cluster mass, which are of unparalleled importance to cosmology (e.g., Bahcall 1995). They will also reflect physical processes that have played a crucial role in the thermal and dynamical evolution of the gas. In addition to gravitation, hydrodynamics, and shock heating, such processes may include radiative cooling, heat conduction, and feedback from star formation.

One of the central questions about the cluster gas structure involves the presence of a core. Observations have revealed that the gas density profile has a distinct core, inside of which density is nearly constant. Gravitational N-body simulations have demonstrated that gravity alone cannot produce such a core in an object formed as a result of hierarchical structure formation; halos formed in high-resolution N-body simulations have density profiles with significant slope toward the center up to the resolution limit (Navarro, Frenk, and White 1996, 1997; Fukushige and Makino 1997; Moore et al. 1998). For example, Navarro, Frenk, and White (1996, 1997) found that the density profiles of halos with a wide range of masses can be fitted by

$$\rho(r) = \frac{\rho_c}{(r/r_s)(1 + r/r_s)^2} \quad (1)$$

(hereafter referred to as the NFW profile), with ρ_c and r_s being the fitting parameters. In the NFW profile, gas temperature would approach zero in a cluster's central regions ($T \propto r$) were it to have the same profile as dark matter. While this model does produce a convergent X-ray luminosity, the temperature structure is different from what is observed. It follows that processes other than gravity are responsible for the formation of the cores. Makino, Sasaki and Suto (1998) pointed out that the gas distribution develops a core in a dark matter halo having a central cusp (e.g., the NFW profile) if the gas is isothermal and in hydrostatic equilibrium. Even if the gas obeys a less stringent limit of constant entropy ($T/n^{2/3} \rightarrow \text{const}$), it would avoid a central cusp and have an apparently constant-density, constant-temperature core. But it is not evident what physical mechanisms could enforce either isothermality or isentropy.

Many authors have studied the evolution of clusters using simulations that include hydrodynamics (Evrard 1990; Thomas and Couchman 1992; Katz and White 1993; Bryan et al. 1994a, 1994b; Kang et al. 1994; Navarro, Frenk, and White 1995; Bartelmann and Steinmetz 1996; Bryan and Norman 1997, 1998; Eke, Navarro, and Frenk 1998; Pen 1998; Yoshikawa, Itoh, and Suto 1998). In general these simulations have succeeded in producing clusters that have cores similar to those observed. However, the situation is far from satisfactory for at least two reasons. First, artificial two-body relaxation may affect the dynamics, especially in the central region. Indeed, Steinmetz and White (1997) showed that this effect gives rise to artificial energy transfer from dark matter to gas. Both spatial and mass resolutions are only marginally adequate in most published works. Second, almost none of the simulations include radiative cooling of gas. Although cooling is probably unimportant in the outer part of a cluster (Sarazin 1986), it may affect the dynamics in the central region.

This work is an investigation of cluster gas using hydrodynamic simulations that attempt to address these limitations. First, we minimize two-body relaxation effects for a given computational cost by employing a multiresolution technique that enables us to improve resolution only inside the clusters where we really need high resolution. Second, we include cooling due to bremsstrahlung, which dominates cooling of gas at above $\gtrsim 10^7$ K. We ignore line cooling, but this is not a serious problem because we focus our attention on X-ray-emitting gas. A practical reason for ignoring line cooling is that doing so enables us to avoid very short timescales in moderate temperature ($10^4 - 10^6$ K), high density regions. Allowing for line cooling would strengthen the conclusions of this paper.

We organize the rest of the paper as follows. In § 2 we describe the method and parameters of the simulations. We present the results in § 3. As we will see, the most important result is that cooling and increased resolution give rise to a density profile of the gas that rises steeply toward the center and consequently produces excessive X-ray luminosity. In § 4 we discuss the implications of our results in connection with physical processes that are still missing in the simulations. In § 5 we give our conclusions.

2. Simulations

We work with a cold dark matter-dominated universe with $h = 0.6$, $\Omega_0 = 1$, $\Lambda = 0$, $\Omega_b = 0.07$, $n_{\text{spect}} = 0.81$, and $\sigma_8 = 0.50$, where h is the Hubble constant in units of $100 \text{ km s}^{-1} \text{ Mpc}^{-1}$, Ω_0 is the cosmological density parameter, Λ is the cosmological constant, Ω_b is the baryon density parameter, n_{spect} is the power-law index of the primordial density fluctuations, and σ_8 is the rms density fluctuations on $8 h^{-1} \text{ Mpc}$ scale.

These parameters are chosen so that the universe is at least marginally consistent with all of the following observations: the amplitude of cosmic microwave background anisotropies observed by COBE, the observational bound on the Hubble constant, the abundance of light elements, the baryon fraction in clusters, the number density of clusters, and the age of the globular clusters. The model is similar to the tilted cold dark matter (TCDM) model of Cen and Ostriker (1993).

We employ a cosmological N-body + smoothed particle hydrodynamics (SPH) code (see e.g. Monaghan 1992 for a review of SPH).

The N-body part of the code uses the Barnes-Hut (1986) tree algorithm and is described in Sugimoto et al. (1991). The SPH part of the code is described in Sugimoto (1992). Overall, the code is similar to the one described in Katz, Weinberg, and Hernquist (1996). An application of the earlier version of the code is in Sugimoto (1994, 1995).

We carry out a multiresolution simulation that allows us to achieve high resolution only inside the clusters. We prepare two sets of initial conditions with different mass resolution in a cubic box with comoving size $L = 42 h^{-1} \text{ Mpc}$. These sets have exactly the same realization, up to the

Nyquist wavenumber corresponding to the lower resolution, of the theoretical power spectrum of density fluctuations at $z = 19$. The number of particles in the higher resolution realization is 8 times that in the lower resolution one. In each realization we assign to all particles the same gravitational softening length ε , which is fixed in the comoving coordinates and is equal to 0.1 times the mean interparticle separation of dark matter particles. The initial gas temperature is set to 10^4 K. Then we use the following two-step procedure. First, we evolve the system from the lower resolution realization. When the low-resolution (LR) run has been carried out up to the present epoch we identify cluster centers. Then we come back to the initial distribution of particles and identify those regions that will end up with overdensity larger than 140 around the cluster centers. We replace the particles in the identified regions with those in the high-resolution realization. Then, starting from this initial condition, we run the second simulation, which is hereafter referred to as the multiresolution (MR) run. Katz and White (1993) and Navarro, Frenk, and White (1996, 1997) used a similar method to construct initial conditions with variable resolution.

The ratio of the number of gas particles to that of dark matter particles is always set as 1/8. Thus in either the low-resolution or high-resolution realizations, the masses of gas particles, m_g , and dark matter particles, m_d , are comparable ($m_g/m_d = 0.6$). Since two-body relaxation time is inversely proportional to $\max(m_g, m_d)$, it is maximized when $m_g = m_d$ under the condition that the available CPU time is fixed. Thus, with the available CPU cost, the artificial two-body effect is significantly reduced compared to when we used an equal number of gas and dark matter particles, as has been done in most previous work. Indeed, the mass of a dark matter particle for the high-resolution realization, $1.5 \times 10^{10} M_\odot$, is less than one-third of the upper bound for two-body heating to be subdominant (Steinmetz and White 1997) for the cluster that is mainly discussed in the following sections.

We allow each particle to have its own time step. The time step of each particle satisfies $\Delta t = (\Delta t)_{\text{sys}}/2^{n_{\text{step}}}$, where $(\Delta t)_{\text{sys}} = 2.4 \times 10^6$ yr. The time-step index n_{step} , which is a nonnegative integer, is chosen so that the following three conditions are satisfied: (i) the Courant condition is satisfied with the Courant number taken to be 0.3 (Katz, Weinberg, and Hernquist 1996), (ii) expected relative change in the internal energy within a time step does not exceed 0.05, and (iii) expected change in position within a time step does not exceed 0.05ε . The parameters for the simulations are summarized in Table 1.

Bremsstrahlung cooling is included in the simulations. Throughout this paper we assume the mass fraction of helium, Y , to be 0.24 and the effect of metals to be negligible, and we use the approximation that $\bar{g} = 1.2$, where \bar{g} is the frequency averaged Gaunt factor. Then bremsstrahlung emissivity is given by

$$\Lambda_B = 5.2 \times 10^{-28} T^{1/2} n^2 \text{ ergs s}^{-1} \text{ cm}^{-3}, \quad (2)$$

where the gas temperature T is in units of K and the gas density n is in units of cm^{-3} (Rybicki and Lightman 1979).

Table 1: Simulation parameters

Run	Resolution ^a	N_g ^b	N_d ^c	$m_g(M_\odot)$ ^d	$m_d(M_\odot)$ ^e	$\varepsilon(h^{-1}\text{kpc})$ ^f	$h_{\min}(h^{-1}\text{kpc})$ ^g
LR	low	32,768	262,144	7.3×10^{10}	1.2×10^{11}	66	66
MR	low	27,962	223,696	7.3×10^{10}	1.2×10^{11}	66	66
MR	high	38,448	307,584	9.2×10^9	1.5×10^{10}	33	33

^aIn run LR, the entire volume is represented by low-resolution particles. In run MR, those regions which will end up in clusters are represented by high-resolution particles, and the remainder of the volume by low-resolution particles.

^bThe number of gas particles.

^cThe number of dark matter particles.

^dThe mass of a gas particle.

^eThe mass of a dark matter particle.

^fGravitational softening length.

^gMinimum smoothing length of gas particles.

3. Results

In this section we present results of the simulations. We have obtained 12 clusters with $M_A \geq 2 \times 10^{14} M_\odot$, where M_A is the total mass inside a radius of $1.5h^{-1}\text{Mpc}$. We have identified these clusters in the following way. First, we extract gas particles with gas density larger than 10^{-4}cm^{-3} out of the whole simulation. Next we group these gas particles using the conventional friends-of-friends algorithm, connecting particles with separation smaller than 0.2 times the mean interparticle separation. We find the center of mass of each group. Then we come back to the entire simulation and extract a spherical region of a radius $2.5h^{-1}\text{Mpc}$, whose center matches the center of mass of the identified group. Finally we redefine the cluster center as the position of the gas particle that has the largest X-ray emissivity.

3.1. Density and temperature profiles

In the remainder of the paper we concentrate, unless otherwise stated, on the richest cluster, with $M_A = 6.9 \times 10^{14} M_\odot$. The half-mass velocity dispersion is 790 km s^{-1} , and the cluster is in the range of normal X-ray-emitting clusters. Figure 1 shows the contour of the column density distribution of gas and dark matter projected on a plane in runs LR and MR. The difference for the two runs is already manifest, especially in the gas distribution, despite the fact that the

only difference in the two runs is the resolution. In run MR the density profile is much more centrally concentrated. Moreover, the cluster in run MR has two distinct subclumps, which are not apparent in run LR.

The difference is also clear in Figure 2, which shows total mass density ρ , gas density n , and temperature T , averaged over a spherical shell, as functions of the radius. In run LR, the logarithmic slope of the total mass density profile gradually changes from ~ -3 in the outer part to ~ -1 in the inner part, i.e., the simulation fits the NFW profile (eq. [1]).

The gas density profile in run LR does not fit the NFW profile but is well fitted by the observationally motivated β profile:

$$n(r) = n_0 \left[1 + \left(\frac{r}{r_c} \right)^2 \right]^{-3\beta/2}, \quad (3)$$

with $n_0 = 5.4 \times 10^{-3} \text{ cm}^{-3}$, $r_c = 140h^{-1}\text{kpc}$, and $\beta = 0.75$. The gas is nearly isothermal with $T = (3-4) \times 10^7 \text{ K}$ in run LR. The X-ray luminosity in this run is $1.9 \times 10^{44} \text{ ergs s}^{-1}$ and is in the normal range observed. This run has resolution and other properties typical of high-resolution numerical simulations of hydrodynamical cosmology. If we had stopped our work at this point, we would have concluded that there was a good correspondence between observation and theory.

In contrast, in the higher resolution run MR the total mass density profile shows a steeper rise toward the center than in run LR. The gas density profile also shows a steep rise toward the center and cannot be fitted at all by the β profile. The temperature in run MR significantly drops toward the center. There is a sharp peak in the gas density profile and drop in the temperature profile at $r \sim 0.3h^{-1}\text{Mpc}$; this corresponds to the smaller subclump seen in Figure 1. These results in run MR can naturally be interpreted as cooling of gas having decreased the temperature and increased the gas density in the central part of the subclumps.

No observed clusters resemble the simulated cluster in run MR. The X-ray intensity is smooth in the central region in roughly half of the observed clusters, which implies that the gas density is nearly constant. The remainder of the clusters do show a peak in X-ray emission, which is claimed to be a feature of a cooling flow (Fabian, Nulsen, and Canizares 1991). However, the inferred gas density at the center of “cooling-flow” clusters is much smaller than in our simulated cluster. There is also a discrepancy between the simulation and the observations in the total X-ray luminosity. The bolometric luminosity L_{bol} of the cluster in run MR is $7.4 \times 10^{45} \text{ ergs s}^{-1}$, far too high for a cluster with temperature $\sim 3 \text{ keV}$; typically $L_{\text{bol}} \sim 10^{44} \text{ ergs s}^{-1}$ for observed clusters with this gas temperature, and none of these have bolometric luminosity exceeding $10^{45} \text{ ergs s}^{-1}$ (David et al. 1993).

We have seen that as a result of increasing the resolution the simulated cluster has moved farther from the observed ones. This is probably because cooling becomes too efficient. The origin of this discrepancy is discussed in § 4.

In general, the other 11 clusters in the higher resolution run have steep gas density profiles

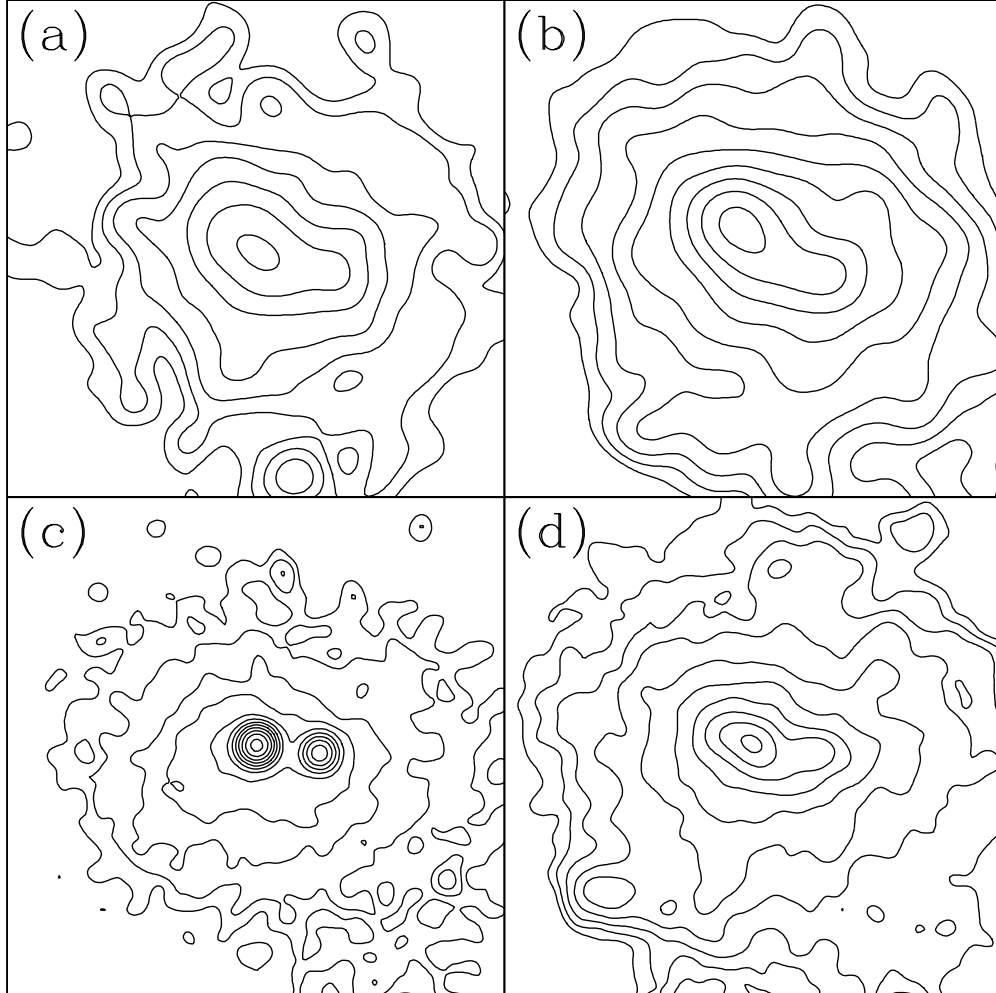


Fig. 1.— Contours of the column density Σ of the richest cluster in the simulation, projected on a plane. The neighboring contour lines correspond to increments of 0.2 in $\log \Sigma$. (a) Column density of the gas in run LR. The contour line that is nearest to the cluster center corresponds to $\Sigma = 10^{-2.6} \text{ g cm}^{-2}$. (b) Column density of the dark matter in run LR. The contour line nearest to the cluster center corresponds to $\Sigma = 10^{-1.4} \text{ g cm}^{-2}$. (c) Column density of the gas in run MR. The contour line nearest to the cluster center corresponds to $\Sigma = 10^{-1.6} \text{ g cm}^{-2}$. (d) Column density of the dark matter in run MR. The contour line nearest to the cluster center corresponds to $\Sigma = 10^{-1.2} \text{ g cm}^{-2}$.

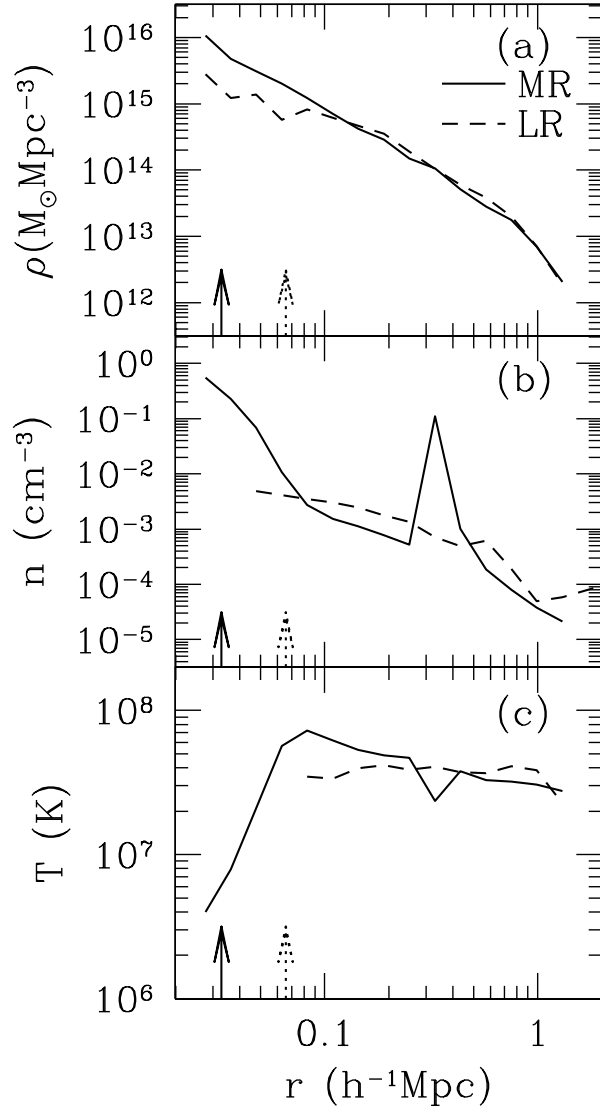


Fig. 2.— Profiles of (a) total mass density, (b) gas density, and (c) temperature in the cluster in runs MR (*solid line*) and LR (*dashed line*). The abscissa is the physical radius. The solid and dotted vertical arrows indicate the gravitational softening length ϵ for runs MR and LR, respectively.

in the central part, similar to the richest cluster. The central density of six of them is greater than 10^{-1}cm^{-3} , and two of them have bolometric luminosity exceeding $10^{45}\text{ergs s}^{-1}$ although they have velocity dispersion of only $500\text{--}600\text{ km s}^{-1}$, considerably smaller than the richest one. Thus the properties of the richest cluster discussed above are not to be attributed to a particular initial condition.

3.2. Evolution

Next we examine the time evolution of the cluster in run MR. Figure 3 shows the total mass density, gas density, and temperature profiles at various redshifts. The temperature increases at any radius from $z = 1.4$ to $z = 0.7$, but at $z \sim 0.7$ the temperature in the central part begins to decrease, and it keeps falling up to $z = 0$. The gas density in the central part increases rapidly from $z \sim 0.7$ to $z = 0$. We also notice that the smaller subclump is approaching the main subclump. These results support our view in the previous subsection that cooling has resulted in a rise in the gas density profile toward the center. On the other hand, the total mass density profile in the central part is already quite steep at $z = 1.4$. This indicates that the steeper rise in run MR than in run LR is a consequence not of the effectiveness of cooling but of the improved accuracy in following the evolution of the dark matter. As some authors have pointed out (Fukushige and Makino 1997; Moore et al. 1998), the “universal” density profile of dark halos claimed by Navarro, Frenk, and White (1996, 1997, eq. [1]) is still a controversial issue and may depend on numerical resolution. Clearly, our higher resolution run allowed the central density to reach higher levels than the lower resolution run even in the absence of cooling. But then, in run MR the density reached a level where the cooling time became short enough for the classical isobaric radiative cooling instability to begin. Allowance for metal-line cooling would have increased the radiative losses by about a factor of 2 and would have accelerated the trends noted.

We find that the cooling time in run LR is greater than the Hubble time up to the resolution limit. Therefore the main reason for the inefficiency of cooling in run LR is simply that the achieved density is not high enough, although two-body heating (Steinmetz and White 1997) may have played an additional role in preventing the gas from cooling.

3.3. Timescales

Now we investigate various timescales in the simulation both as a function of radius and as a function of time. The purpose is to confirm that no obvious numerical artifacts are invalidating the results of the present simulations and that cooling is indeed what has caused the gas density profile to rise steeply toward the center.

The timescales we are going to discuss are the following:

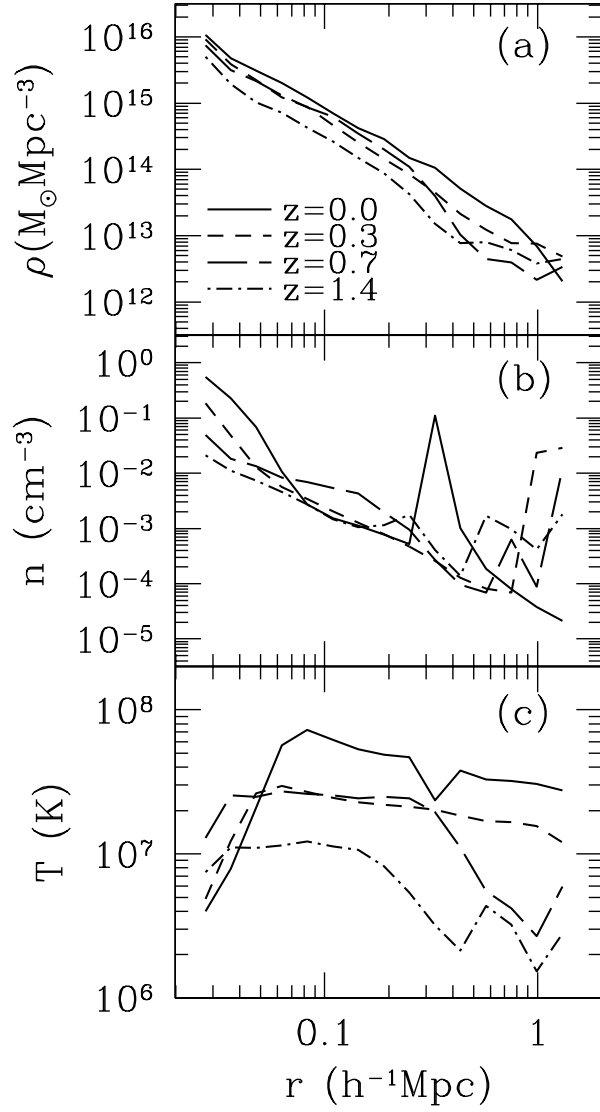


Fig. 3.— Profiles of (a) total mass density, (b) gas density, and (c) temperature in the cluster in run MR at $z = 1.4$ (*dot-dashed line*), $z = 0.7$ (*long-dashed line*), $z = 0.3$ (*short-dashed line*) and $z = 0$ (*solid line*). The abscissa is the physical radius.

- Dynamical time:

$$t_{\text{dyn}} \equiv \frac{1}{(G\rho)^{1/2}}. \quad (4)$$

- Relaxation time due to artificial two-body effects:

$$t_{\text{relax}} \equiv 0.34 \frac{\sigma^3}{G^2 m_d \rho (\ln \Lambda)_g} \quad (5)$$

(Binney and Tremaine 1987), where σ is the one-dimensional velocity dispersion and $(\ln \Lambda)_g$ is the Coulomb logarithm associated with gravitational interaction, which we estimate by

$$(\ln \Lambda)_g = \ln(r/\varepsilon). \quad (6)$$

- Cooling time:

$$\begin{aligned} t_{\text{cool}} &\equiv \frac{5 nkT}{2 \Lambda_{\text{cool}}} \\ &= 2.1 \times 10^4 n^{-1} T^{1/2} \text{ yr}, \end{aligned} \quad (7)$$

where k is Boltzmann's constant and n and T in the second line are in cgs units.

- Hubble time (3/2 times the age of the universe):

$$t_H = H_0^{-1} (1+z)^{-3/2}. \quad (8)$$

Figure 4 shows these timescales as functions of radius at various redshifts. Also shown is the heat conduction time t_{cond} , which will be considered in § 4. From Figure 4 several points become clear:

- (i) All of the relevant timescales are always larger than $(\Delta t)_{\text{sys}}$ in any part of the cluster. This assures that the time step adopted in our simulation is short enough to accurately follow the evolution, even where cooling is taking place.
- (ii) The relaxation time t_{relax} is always much greater than the Hubble time t_H . This means that the mass resolution is high enough that the MR simulation is not being affected by artificial two-body relaxation.
- (iii) The cooling time t_{cool} becomes shorter than t_H at $z \sim 0.7$ both at the center of the main clump and at the center of the smaller subclump. This implies that cooling is certainly affecting the thermal and dynamical evolution of gas.

4. Discussion

We have seen that the high-resolution simulated clusters do not develop a core in the gas distribution as is observed. Rather, the gas density increases steeply toward the center. In this

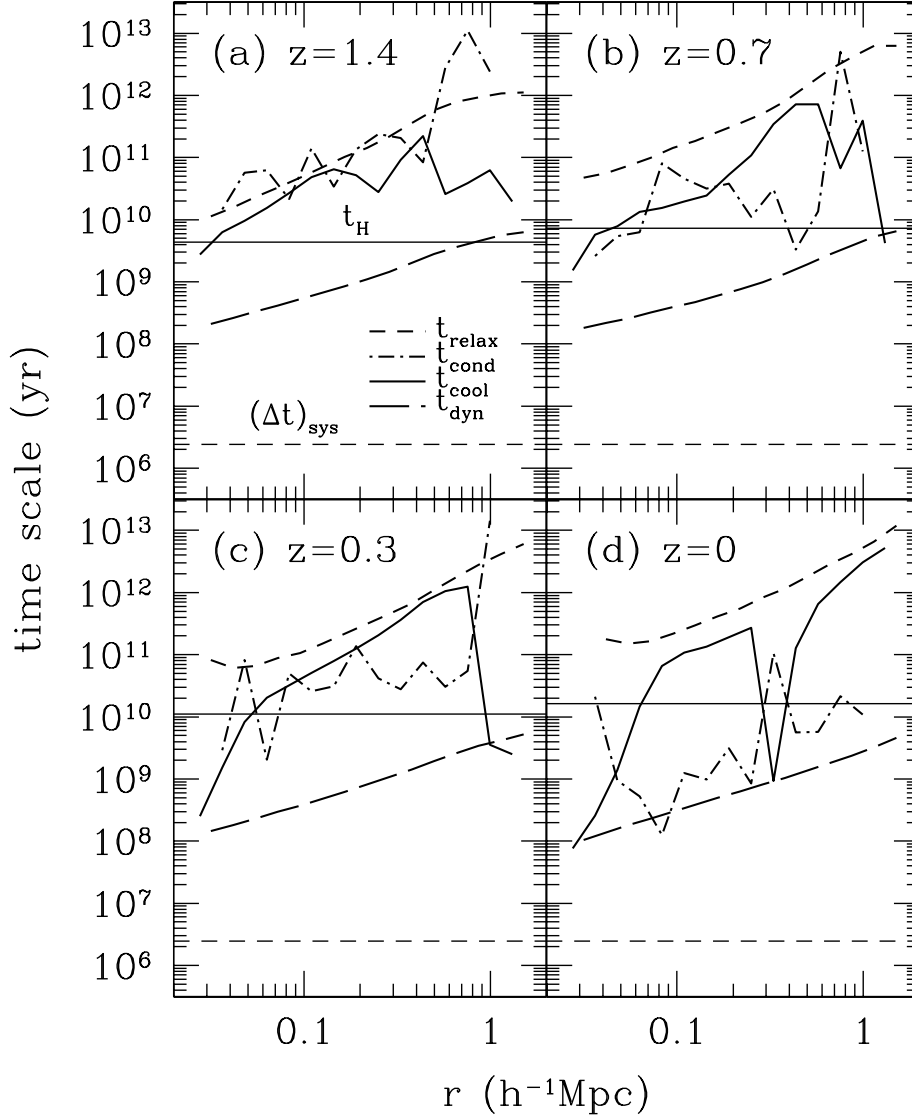


Fig. 4.— Dynamical time (*long-dashed line*), two-body relaxation time (*short-dashed line*), cooling time (*solid line*) and conduction time (*dot-dashed line*) in the cluster in run MR at (a) $z = 1.4$, (b) $z = 0.7$, (c) $z = 0.3$, and (d) $z = 0$. The horizontal thin solid line is the Hubble time, and the horizontal thin dashed line is the system time step $(\Delta t)_{\text{sys}}$. The abscissa is the physical radius.

section we discuss what is responsible for the discrepancy between the simulated and observed clusters.

To begin with, let us consider numerical resolution. In fact it is uncertain whether we have yet achieved sufficient mass and spatial resolution to accurately follow the evolution of the gas density profile with bremsstrahlung cooling included. However, even if our resolution is insufficient, this is probably not the cause of the discrepancy. If we had better resolution, we would be able to follow density inhomogeneities on small scales more accurately. Since the cooling rate is proportional to the square of the gas density, this would have resulted in more efficient cooling, and hence an even steeper gas density profile toward the center.

In the remainder of the paper we discuss the effects of (1) changing the cosmological parameters, (2) heat conduction, and (3) heating of gas due to supernovae (SNe).

4.1. Cosmological parameters

There are now a variety of observations that constrain the cosmological parameters, such as h , Ω_0 , Λ_0 , Ω_b , σ_8 , and Ω_ν , where Ω_ν is the density of an additional hot dark matter component in units of the critical density. It seems reasonable to expect that changing these parameters would not largely alter the cluster density profile if the parameters were constrained to satisfy observational requirements.

Since hot dark matter does not cluster on small scales, adding a hot dark matter component will tend to make the central density profile shallower. This may push the simulation result closer to those of the observations. However, too much of a hot dark matter component results in failure to form objects at a high enough redshift, and at the level of currently considered viable models, $\Omega_\nu = 0.2$ (Klypin et al. 1995), the effects on cluster properties are not large.

4.2. Heat conduction

If heat conduction takes place in a timescale shorter than cooling time, it will tend to stabilize the gas, perhaps resulting in nearly isothermal gas with a smooth density profile near the center. We estimate the heat conduction time t_{cond} in the simulated cluster by

$$t_{\text{cond}} \equiv \frac{5}{2} \frac{nkT}{|\nabla \cdot (\kappa \nabla T)|}. \quad (9)$$

Here

$$\kappa = 1.8 \times 10^{-5} T^{5/2} (\ln \Lambda)_e^{-1} \quad \text{ergs s}^{-1} \text{cm}^{-1} \text{K}^{-1} \quad (10)$$

is the heat conductivity, where the Coulomb logarithm $(\ln \Lambda)_e$, associated with electrostatic interactions between electrons, is

$$(\ln \Lambda)_e = 37.8 + \ln \left[\left(\frac{T}{10^8 \text{K}} \right) \left(\frac{n_e}{10^{-3} \text{cm}^{-3}} \right)^{-1/2} \right], \quad (11)$$

with n_e being the electron number density (Sarazin 1986).

In Figure 4 we plot t_{cond} as a function of radius. Just outside the radius where t_{cool} begins to drop below t_H , t_{cond} becomes smaller than both t_{cool} and t_H . This implies that heat conduction may be efficient enough to prevent the inner gas from cooling.

Thus heat conduction may have played a crucial role in the formation of the core in spatial distribution of gas in clusters. However, observations suggest that cluster gas is associated with a weak magnetic field, which is tangled on a scale ~ 10 kpc. If this is the case, the heat conductivity may be suppressed by more than 2 orders of magnitude (Krommes, Oberman and Kleva 1983; Chandran and Cowley 1998), and conduction may not be able to prevent gas from cooling. At present, both the physical state of the magnetic field in clusters (if existent) and the extent to which it can suppress conduction remain open questions.

4.3. SN heating

Heat input to cluster gas from supernova (SN) explosions occurring in cluster galaxies is another process that may be responsible for the discrepancy between the simulation and observations. SN heating will raise the entropy and may lower the density and raise the temperature of the gas so efficiently as to prevent it from cooling. If this is the case, then the gas distribution may develop a core similar to the observed ones.

To assess this effect, we estimate entropy increase due to SN heating, using observed iron abundance. Heat that has been ejected from SNe per unit gas mass can be estimated as

$$\Delta q = 2.0 \times 10^{-3} \chi \left[f_{\text{I}} \frac{E_{\text{I}}}{M_{\text{Fe,I}}} + (1 - f_{\text{I}}) \frac{E_{\text{II}}}{M_{\text{Fe,II}}} \right], \quad (12)$$

where χ is the iron abundance in units of solar abundance, E_{I} and $M_{\text{Fe,I}}$ are the explosion energy and ejected iron mass per Type Ia SN, E_{II} and $M_{\text{Fe,II}}$ are the same for Type II SN, and f_{I} is the fraction of iron that has been produced by Type I SNe. We adopt

$$E_{\text{I}} = 1.3 \times 10^{51} \text{ ergs}, \quad (13)$$

$$M_{\text{Fe,I}} = 0.744 M_{\odot}, \quad (14)$$

$$E_{\text{II}} = 1 \times 10^{51} \text{ ergs}, \quad (15)$$

and

$$M_{\text{Fe,II}} = 0.038 M_{\odot} \quad (16)$$

(Nomoto, Thielemann, and Yokoi 1984; Thielemann, Nomoto, and Hashimoto 1993). The value of $M_{\text{Fe,II}}$ is an average over the progenitor mass weighted with the Salpeter initial mass function. The fraction f_{I} can be estimated from abundance ratios, but there is still considerable uncertainty (Gibson, Loewenstein, and Mushotzky 1997). We adopt $f_{\text{I}} = 0.5$. We take the AWM7 cluster as an example (Ezawa et al. 1997) and fit the observed iron abundance as a function of radius r to the following profile:

$$\chi = 0.58 \left[1 + \left(\frac{r}{0.058 h^{-1} \text{Mpc}} \right)^2 \right]^{-0.3}. \quad (17)$$

If the SN rate is nearly constant up to the present epoch, we can approximate the entropy increase due to SNe, $(\Delta s)_{\text{SN}}$, fairly well by $\Delta q/T$. Figure 5a shows $(\Delta s)_{\text{SN}}$ as a function of radius r . We express the entropy in units of $3k/(2\mu m_p)$, where μ is the mean molecular weight and m_p is the proton mass. We also plot $s - s_i$, where s_i and s are the entropy at the initial and present epochs in the simulation. In the innermost region of the cluster, $(\Delta s)_{\text{SN}}$ exceeds $s - s_i$. This implies that heating due to SNe can significantly alter the thermal evolution of the gas in the central region.

If the SN rate was much larger at $z \gtrsim 1$ than at $z \sim 0$, as is suggested by apparent lack of evolution in the iron abundance in clusters toward higher redshifts (Mushotzky and Loewenstein 1997), then the above estimate of $(\Delta s)_{\text{SN}}$ is a poor approximation in the central region because the temperature has significantly decreased toward the present epoch. In this case, it is better to assess the effect at a higher redshift. Figure 5b shows $(\Delta s)_{\text{SN}}$ and $s - s_i$ at $z = 0.7$. This time $(\Delta s)_{\text{SN}}$ is smaller than $s - s_i$ everywhere. This indicates that SN heating should have little effect in cases in which SN activities in the cluster continued at a nearly constant rate up to $z \sim 0.7$ and have essentially stopped after that. Finally, we can consider the case where most of the entropy was injected within the first $\sim 10^9$ yr. Then the effect should be very significant, because the gas temperature was relatively low: we find $n \sim 1 \times 10^{-3} \text{cm}^{-3}$ and $T \sim 5 \times 10^5 \text{K}$ at the density peak of a protocluster at $z = 5$, which will end up in the central region of the cluster at $z = 0$. Hence $(\Delta s)_{\text{SN}}$ is estimated as ~ 80 and far exceeds $s - s_i \sim 4$.

Thus SN heating can be an important factor in the formation of the core in the gas distribution, but the effect is strongly dependent on, among other things, the detailed star formation history inside the cluster.

5. Conclusions

Finally let us briefly summarize our conclusions.

1. Our multiresolution simulation has followed with reasonable accuracy the evolution of gas and dark matter in a typical cluster under the influence of bremsstrahlung cooling as well as gravity and hydrodynamics.

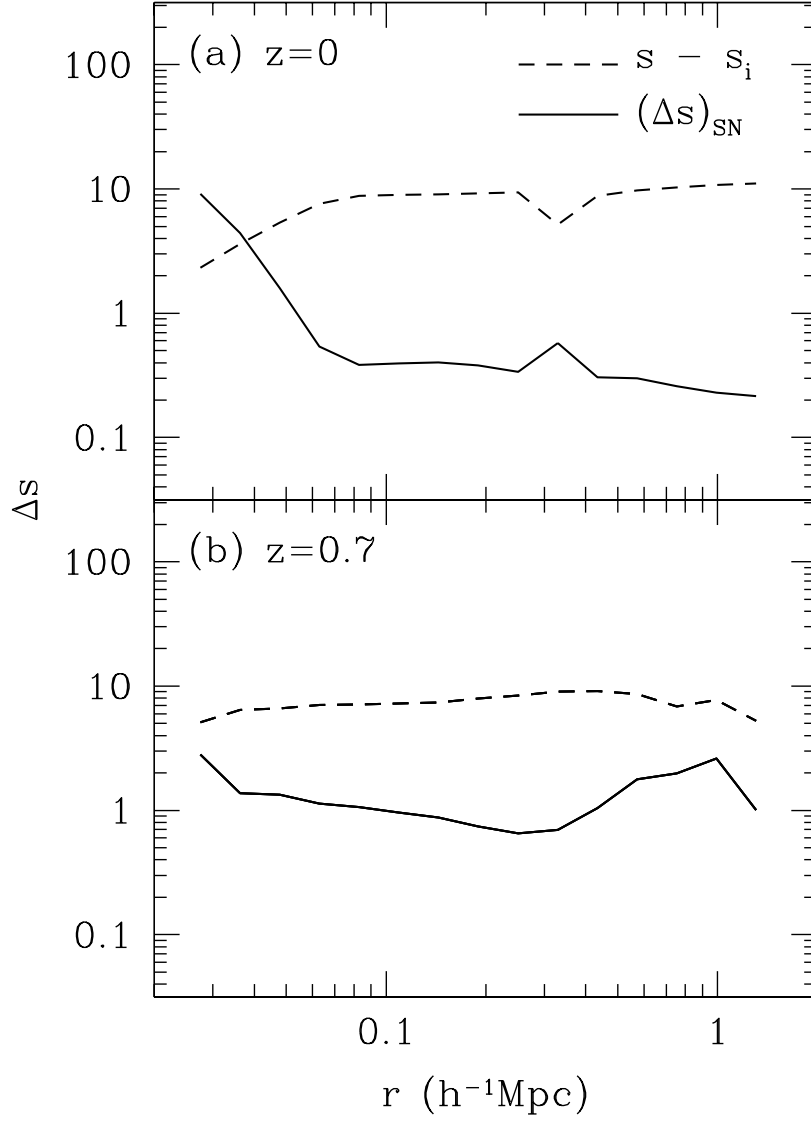


Fig. 5.— Entropy increase $(\Delta s)_{\text{SN}}$ due to supernovae (*solid line*), and entropy change $s - s_i$ in the simulation (*dashed line*). (a) $z = 0$. (b) $z = 0.7$.

2. The high resolution simulation resulted in a gas density profile steeply rising toward the center, with consequent very high X-ray luminosity; however, these properties are not observed.
3. Heat conduction and SN heating are among the processes that may account for the discrepancy. Had we allowed for their likely importance in the real world we might have been able to recover the observed gas density profile. In a future work we will examine their effects by directly incorporating them into the simulation.

T. S. acknowledges support from Research Fellowships of the Japan Society for the Promotion of Science. J. P. O. was supported by NASA grant NAG 5-2759 and NSF grants AST 93-18185, ACI 96-19019 (PACI Subaward No. 766), and AST 94-24416. Numerical computation was carried out on VPP/300 and VX/4R at the Astronomical Data Analysis Center of the National Astronomical Observatory in Japan, as well as on VX/4R at RESCEU (Research Center for the Early Universe, the University of Tokyo).

REFERENCES

- Bahcall, N. A. 1995, in *Large Scale Structure in the Universe*, ed. J. P. Mücke, S. Gottlöber and V. Müller (Singapore: World Scientific), 209
- Barnes, J. and Hut, P. 1986, *Nature*, 324, 446
- Bartelmann, M., and Steinmetz, M. 1996, *MNRAS*, 283, 431
- Binney, J., and Tremaine, S. 1987, *Galactic Dynamics* (Princeton: Princeton Univ. Press)
- Bryan, G. L., Cen, R. Y., Norman, M. L., Ostriker, J. P., and Stone, J. M. 1994a, *ApJ*, 428, 405
- Bryan, G. L., Klypin, A., Loken, C., Norman, M. L., and Burns, J. O. 1994b, *ApJ*, 437, L5
- Bryan, G. L., and Norman, M. L. 1997, in *ASP Conf. Ser. 123*, 12th “Kingston Meeting”: *Computational Astrophysics*, ed. D. A. Clarke and M. J. West (San Francisco: ASP), 363
- Bryan, G. L., and Norman, M. L. 1998, *ApJ*, 495, 80
- Cen, R. Y., and Ostriker, J. P. 1993, *ApJ*, 414, 407
- Chandran, B. D. G., and Cowley, S. C. 1998, *Phys. Rev. Lett.*, 80, 3077
- David, L. P., Slyz, A., Jones, C., Forman, W., Vrtilik, S. D., and Arnaud, K. A. 1993, *ApJ*, 412, 479
- Eke, V. R., Navarro, J. F., and Frenk, C. S. 1998, *ApJ*, 503, 569
- Evrard, A. E. 1990, *ApJ*, 363, 349
- Ezawa, H., Fukazawa, Y., Makishima, K., Ohashi, T., Takahara, F., Xu, H., and Yamasaki, N. Y. 1997, *ApJ*, 490, L33
- Fabian, A. C., Nulsen, P. E. J., and Canizares, C. R. 1991, *A&A Rev.*, 2, 191
- Fukushige, T., and Makino, J. 1997, *ApJ*, 477, L9
- Gibson, B. K., Loewenstein, M., and Mushotzky, R. F. 1997, *MNRAS*, 290, 623
- Kang, H., Cen, R. Y., Ostriker, J. P., and Ryu, D. 1994, *ApJ*, 428, 1
- Katz, N., Weinberg, D. H., and Hernquist, L. 1996, *ApJS*, 105, 19
- Katz, N., and White, S. D. M. 1993, *ApJ*, 412, 455
- Klypin, A., Borgani, S., Holtzman, J., and Primack, J. 1995, *ApJ*, 444, 1
- Krommes, J. A., Oberman, C., and Kleva, R. G. 1983, *J. Plasma Phys.*, 30, 11

- Makino, N., Sasaki, S., and Suto, Y. 1998, *ApJ*, 497, 555
- Monaghan, J. J. 1992, *ARA&A*, 30, 543
- Moore, B., Governato, F., Quinn, T., Stadel, J., and Lake, G. 1998, *ApJ*, 499, L5
- Mushotzky, R. F., and Loewenstein, M. 1997, *ApJ*, 481, L63
- Navarro, J. F., Frenk, C. S., and White, S. D. M. 1995, *MNRAS*, 275, 720
- Navarro, J. F., Frenk, C. S., and White, S. D. M. 1996, *ApJ*, 462, 563
- Navarro, J. F., Frenk, C. S., and White, S. D. M. 1997, *ApJ*, 490, 493
- Nomoto, K., Thielemann, F.-K., and Yokoi, K. 1984, *ApJ*, 286, 644
- Pen, U. 1998, *ApJ*, 498, 60
- Rybicki, G. B., and Lightman, A. P. 1979, *Radiative Processes in Astrophysics* (New York: John Wiley & Sons)
- Sarazin, C. L. 1986, *Rev. Mod. Phys.*, 58, 1
- Steinmetz, M., and White, S. D. M. 1997, *MNRAS*, 288, 545
- Suginohara, T. 1992, Ph. D. thesis, the University of Tokyo
- Suginohara, T. 1994, *PASJ*, 46, 441
- Suginohara, T. 1995, in *Large Scale Structure in the Universe*, ed. J. P. Mücke, S. Gottlöber, and V. Müller (Singapore: World Scientific), 242
- Suginohara, T., Suto, Y., Bouchet, F. R., and Hernquist, L. 1991, *ApJS*, 75, 631
- Thielemann, F.-K., Nomoto, K., and Hashimoto, M. 1993, in *Origin and Evolution of the Elements*, ed. N. Prantzos, E. Vangioni-Flam, and M. Cassé (Cambridge: Cambridge Univ. Press), 297
- Thomas, P. A., and Couchman, H. M. P. 1992, *MNRAS*, 257, 11
- Yoshikawa, K., Itoh, M., and Suto, Y. 1998, *PASJ*, 50, 203